White Rose Research Online

eprints@whiterose.ac.uk
https://eprints.whiterose.ac.uk
Universities of Leeds, Sheffield and York

Deposited via The University of Leeds.

White Rose Research Online URL for this paper:
https://eprints.whiterose.ac.uk/id/eprint/247217/

Version: Supplemental Material

Article:
Li, L., Kumar, S., Moorhouse, T. et al. (Accepted: 2026) Transient epitaxial dynamics and cascade continuity in long-duration terahertz quantum cascade laser growth. Journel of Applied Physics. ISSN: 0021-8979 (In Press)

This is an author produced version of an article accepted for publication in Journal of Applied Physics, made available via the University of Leeds Research Outputs Policy under the terms of the Creative Commons Attribution License (CC-BY), which permits unrestricted use, distribution and reproduction in any medium, provided the original work is properly cited.

Reuse
Items deposited in White Rose Research Online are protected by copyright, with all rights reserved unless indicated otherwise. They may be downloaded and/or printed for private study, or other acts as permitted by national copyright laws. The publisher or other rights holders may allow further reproduction and re-use of the full text version. This is indicated by the licence information on the White Rose Research Online record for the item.

Takedown
If you consider content in White Rose Research Online to be in breach of UK law, please notify us by emailing eprints@whiterose.ac.uk including the URL of the record and the reason for the withdrawal request.

UNIVERSITY OF LEEDS
University of Sheffield
UNIVERSITY of York

Supplementary Material for

"Transient epitaxial dynamics and cascade continuity in long-duration terahertz quantum cascade laser growth"

Lianhe Li[1,*], Sumona Kumar[1], Thomas Moorhouse[1], Minghui You[2], A. Giles Davies[1], Edmund H. Linfield[1]

[1] School of Electronic and Electrical Engineering, University of Leeds, Woodhouse Lane, Leeds LS2 9JT, UK

[2] College of Engineering and Technology, Changchun Normal University, No. 677 Changji beixian, Changchun City, Jilin Province, P.R. China, post code 130032

S1. Pyrometry phase-departure analysis

The in-situ pyrometry signal was acquired using a kSA BandiT pyrometry system at 12.7-s intervals. The signal was then smoothed using a three-point boxcar average for the quantitative phase analysis.

The measured interference oscillations were compared with transfer-matrix-calculated reference trajectories, following the pyrometric modelling approach previously applied to THz QCL growth [1], with the underlying in-situ reflectance modelling formalism described in Ref. [2]. The calculations used here were implemented in Mathcad. The phase departure was determined from the temporal displacement of the experimental pyrometry extrema relative to the corresponding extrema of the calculated constant-growth-rate reference trajectory.

In the Mathcad outputs shown in Figs. S1–S4, the horizontal axis is the time coordinate in seconds, and the vertical axis is the pyrometry interference-signal amplitude. *Shift* denotes the temporal translation applied to the experimental trace to establish its phase origin relative to the calculated reference. The calculated reference trajectory itself remains fixed relative to its time origin. *Gr0* is the Mathcad label for the constant reference growth rate G_r used in Eqs. (S1)–(S3), in μm h^{-1}.

The analysis below proceeds in three stages. Section S1.1 defines the phase departure relative to a constant-growth-rate reference and examines its dependence on the selected reference rate. Section S1.2 describes the piecewise procedure used to estimate interval-averaged effective growth rates when a single constant-rate trajectory no longer describes the full phase evolution. Section S1.3 examines the sensitivity of this estimation to small changes in the assumed constant effective growth rate and to temporal re-referencing.

S1.1 Phase departure relative to a constant-growth-rate reference

Phase departure was determined from the progressive temporal displacement between the experimental pyrometry oscillations and the calculated constant-growth-rate reference trajectory. Within the effective-growth-rate representation used in the transfer-matrix analysis, and with the optical parameters held fixed, the phase departure may be written, to first order and for a constant reference growth rate G_r, as

$$\Delta\varphi_r(t) = K \int_0^t [G(t') - G_r]\, dt', \qquad (S1)$$

where G(t) represents the effective time-dependent growth rate and K is an effective proportionality factor for the optical phase response under the conditions considered here. If a different constant reference growth rate G_r' is selected while retaining the same phase origin, subtraction of the two phase-departure trajectories gives

$$\Delta\varphi_{r'}(t) - \Delta\varphi_r(t) = K\int_0^t (G_r - G_r')\, dt' = K(G_r - G_r')t. \qquad (S2)$$

Thus, changing the constant reference growth rate introduces only a linear contribution to the phase-departure trajectory and cannot itself generate the transient nonlinear features associated with changes in the underlying growth dynamics. Equivalently,

$$d^2\Delta\varphi_r/dt^2 = K\, dG(t)/dt, \qquad (S3)$$

which is independent of the selected constant reference growth rate. Accordingly, within this representation, the characteristic transient or non-monotonic component of the phase-departure evolution is not generated by the choice of constant reference growth rate.

To illustrate the analysis procedure, a structurally simpler reference structure consisting of a 40-nm AlAs layer followed by an approximately 15-μm undoped GaAs layer was selected. Figs. S1–S4 present the long-duration pyrometry trace recorded during the growth of this structure. The analysed portion of the trace corresponds to the extended growth of the GaAs layer without the repeated compositional modulation present in a QCL active region.

The simple layer structure, clear interference contrast, and readily visible accumulated phase departure make this trace particularly well suited for demonstrating the analysis procedure and its sensitivity. For this reference structure, the known GaAs/AlAs layer sequence and corresponding optical parameters were used directly in the transfer-matrix calculation. Its additional role as an independent reference for long-duration transient growth dynamics outside the repeated QCL multilayer architecture is discussed in the main manuscript.

For the QCL analysis, the periodically repeated active-region structure was represented optically by an equivalent low-Al-content AlGaAs medium [1]. The effective Al composition was calculated as the thickness-weighted average over one active-region period, and the corresponding effective refractive index was obtained from the GaAs and AlAs optical parameters using the composition interpolation implemented in the model. This effective optical medium was then used to calculate the reference pyrometry oscillations for a constant growth rate.

Figure S1 shows the pyrometry evolution over essentially the full growth of the GaAs layer, covering a total growth duration of approximately 54,000 s (15 h). This extended observation window spans many successive interference oscillations and provides a sensitive record of the accumulated phase evolution during long-duration growth. It also allows departures from a constant-growth-rate reference, which may emerge only after several hours of otherwise stable growth, to become readily apparent. Good agreement can be obtained over part of the growth, but a systematic phase departure subsequently develops, showing that a single constant-rate trajectory cannot describe the complete experimental phase evolution and motivating the piecewise treatment described in Section S1.2. To illustrate the sensitivity of the comparison to the assumed growth rate, the same temporal translation of the experimental record is applied to two slightly different constant-growth-rate references in Fig. S1. This provides a direct comparison of how a small change in the assumed growth rate affects the long-duration agreement between the experimental and calculated oscillations while the temporal alignment is held fixed. A dedicated sensitivity analysis is presented in Section S1.3.

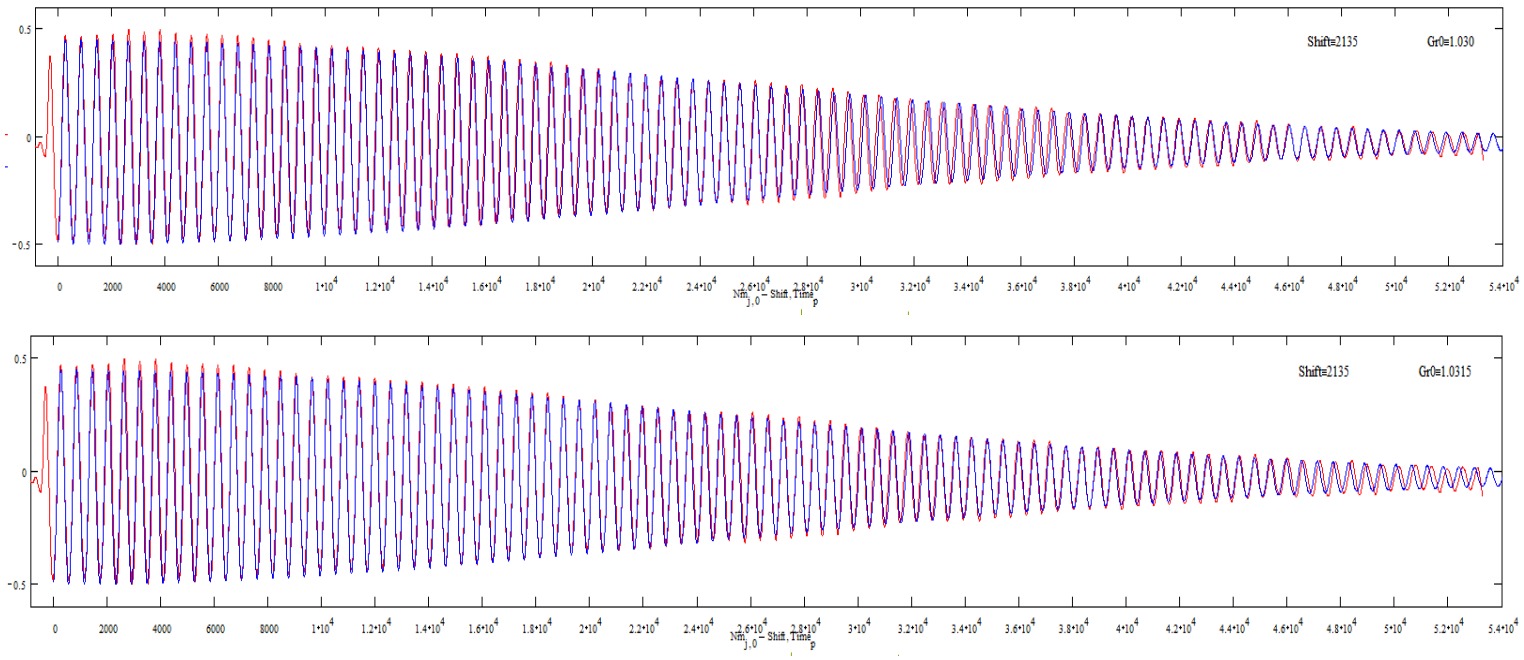


Figure S1. *Long-duration comparison of experimental pyrometry oscillations (red) with transfer-matrix-calculated constant-growth-rate references (blue) for the GaAs reference growth. The upper and lower panels use effective growth rates of 1.0300 and 1.0315 μm h⁻¹, respectively, with the same temporal translation (Shift = 2135 s). A systematic phase departure develops over the extended growth duration, while the two assumed rates produce clearly different long-duration agreement.*

Alt text:

Experimental pyrometry oscillations for a thick-GaAs reference are compared with calculated constant-rate trajectories of 1.0300 and 1.0315 micrometres per hour. A small difference in assumed growth rate produces clearly different long-duration phase agreement.

S1.2 Piecewise estimation of effective growth-rate variation

The inability of a single constant effective growth rate to describe the complete phase evolution motivates a piecewise treatment of the pyrometry record. The accumulated phase departure indicates that the growth evolution departs from that described by a single constant-rate reference. However, because the phase departure at a given time reflects the accumulated preceding growth history, it cannot in general be converted uniquely into a single instantaneous growth-rate deviation.

The experimental and calculated oscillations were therefore compared piecewise. For each comparison interval, the time origin of the calculated reference was kept fixed, while the experimental record was translated along the time axis so that the first selected experimental peak coincided with the corresponding peak of the calculated reference. The assumed constant effective growth rate was then adjusted manually to obtain sustained phase agreement over the subsequent oscillations. During this adjustment, the temporal translation of the experimental record was refined as necessary to maintain coincidence of the initial peak. In this way, the initial peak defines a common phase origin for the comparison, while the assumed growth rate determines the subsequent rate of phase accumulation. When a systematic phase departure developed, a later portion of the experimental record was re-aligned in the same manner to establish a new comparison interval, and a new effective growth rate was determined. This procedure was repeated where necessary for successive portions of the growth. The matching criterion was sustained phase agreement between the experimental and calculated oscillations over multiple successive oscillation periods, rather than agreement at a single point. Figure S2 gives two representative examples of this piecewise procedure. The examples shown in Fig. S2 each extend over a window of approximately 20,000 s (~5.6 h) of the growth record. In the upper panel, sustained phase agreement is maintained for approximately 9,500 s (~2.6 h) before a systematic departure develops; in the lower panel, comparable agreement persists over almost the full window.

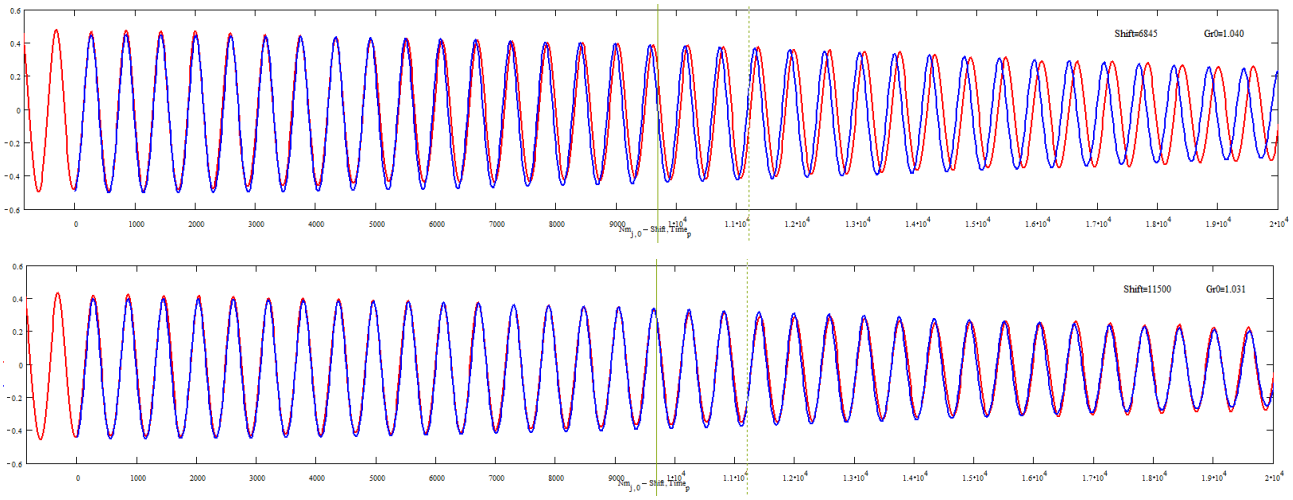


Figure S2. *Representative piecewise comparisons used to estimate interval-averaged effective growth rates. The upper panel uses Shift = 6845 s and an effective growth rate of 1.040 µm h⁻¹; the lower panel uses Shift = 11500 s and 1.031 µm h⁻¹. A systematic phase departure develops in the upper comparison, whereas sustained phase agreement is maintained over most of the lower comparison window.*

Alt text:

Piecewise pyrometry comparisons illustrate interval-averaged growth-rate estimation. One interval develops a systematic phase departure, whereas a later interval fitted with a different effective rate maintains agreement over multiple oscillations.

The values obtained in this way should therefore be interpreted as interval-averaged effective growth rates, rather than as instantaneous growth rates or direct measures of source-flux changes. Each interval is represented by a

single effective constant growth rate that is consistent with sustained phase agreement over that portion of the experimental record.

The interval-dependent differences in effective growth rate are consistent with the coexistence of different effective periodicities indicated by the split high-order HRXRD satellites. However, pyrometry and HRXRD probe the growth history in different ways; the HRXRD components cannot be assigned uniquely to specific depth intervals or temporal stages of the growth, and no one-to-one correspondence is assigned between a particular pyrometry interval and an individual HRXRD component. The quantitative comparison between the pyrometry-derived effective growth-rate difference and the HRXRD-derived effective-period difference is discussed in the main text.

S1.3 Sensitivity of the effective growth-rate estimation

Because the interval-averaged effective growth rates are estimated using a manual, physics-guided comparison of the experimental and calculated phase evolution, the sensitivity of the procedure and its dependence on temporal re-referencing were examined directly in two complementary ways. No formal statistical confidence interval is inferred from this manual matching procedure.

(a) Sensitivity to the assumed effective growth rate

First, the assumed effective growth rate was perturbed while retaining the same temporal translation of the experimental record. As shown in Fig. S3, the calculated traces use the same *Shift* = 12675 s, while the effective growth rate is changed from 1.0305 to 1.0319 μm h^{-1}. The comparison shown in Fig. S3 extends over approximately 25,000 s (~6.9 h). This difference of only 0.0014 μm h^{-1}, corresponding to approximately 0.14%, produces a clearly distinguishable change in the long-duration agreement between the experimental and calculated oscillations, most apparent in the later part of the comparison window. The result demonstrates that the long-duration pyrometry comparison is highly sensitive to small differences in the assumed interval-averaged effective growth rate.

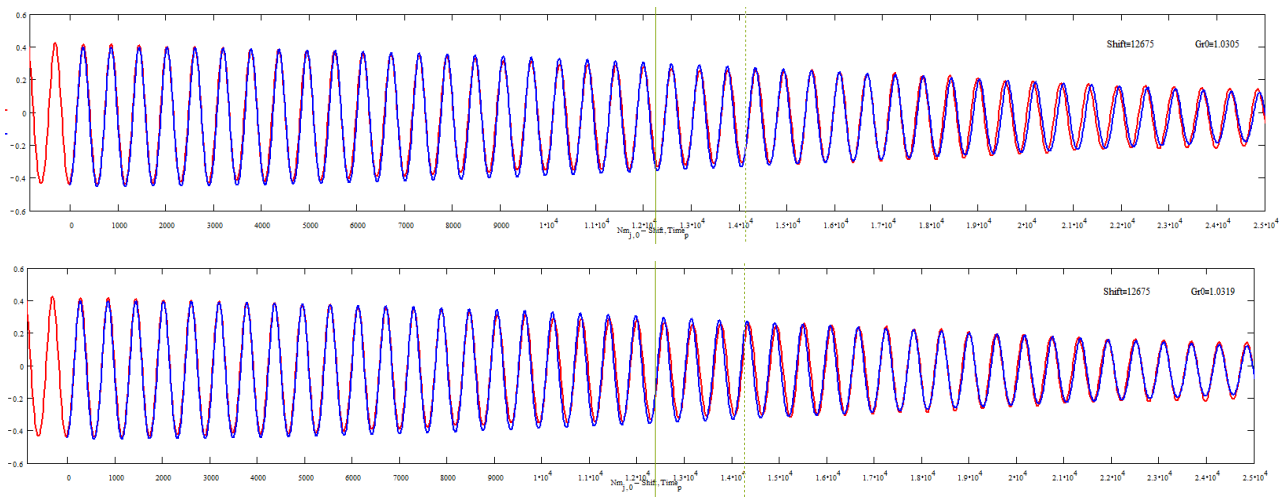


Figure S3. *Sensitivity of the long-duration pyrometry comparison to the assumed effective growth rate. Experimental oscillations (red) are compared with calculated oscillations (blue) using the same Shift = 12675 s and effective growth rates of 1.0305 μm h^{-1} (upper) and 1.0319 μm h^{-1} (lower). The ~0.14% rate difference produces a clearly distinguishable change in the long-duration agreement.*

Alt text:

A sensitivity test compares calculated pyrometry trajectories differing in effective growth rate by approximately 0.14 percent. The small rate change produces a clearly distinguishable difference in long-duration phase agreement.

(b) Sensitivity to the re-referencing position

Second, the assumed effective growth rate was kept unchanged while the temporal translation applied to the experimental record was varied. As shown in Fig. S4, the same effective growth rate of 1.031 μm h^{-1} gives very similar long-duration agreement when *Shift* is changed from 11500 to 12678 s, corresponding to a difference in temporal translation of 1178 s (~19.6 min), or approximately two interference periods. The comparison spans approximately 20,000 s (~5.6 h), providing a multi-hour window over which to assess whether sustained phase agreement is retained after temporal re-referencing by approximately two oscillation periods while the assumed effective growth rate is held fixed. The persistence of long-duration agreement under these two temporal translations indicates that the inferred interval-averaged effective growth rate is not solely a consequence of one particular initial phase alignment. Within the model, with the optical parameters and assumed effective growth rate held fixed, changing *Shift* changes the phase origin of the comparison while leaving the assumed effective growth rate unchanged. Sustained agreement over an extended multi-oscillation interval therefore provides the relevant test of whether the same interval-averaged effective growth rate remains consistent with the experimental phase evolution after temporal re-referencing.

Together, the tests in Figs. S3 and S4 show that the long-duration pyrometry comparison is highly sensitive to small changes in the assumed effective growth rate, while comparable long-duration agreement can be retained under the temporal-translation conditions tested. These tests assess the sensitivity of the piecewise growth-rate estimation and its dependence on temporal re-referencing. However, they are not intended to define a formal statistical uncertainty or confidence interval.

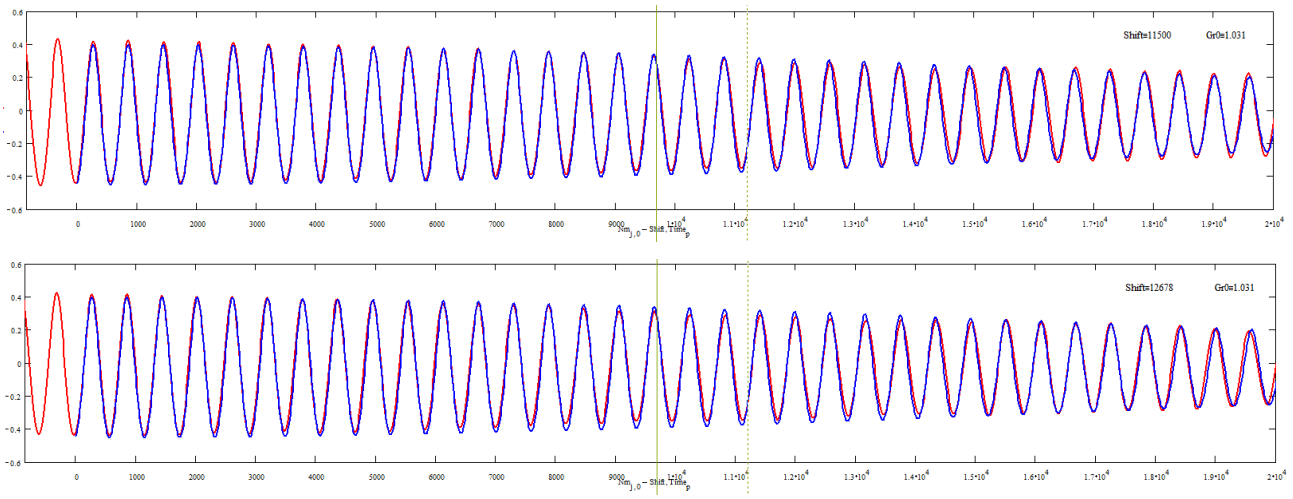


Figure S4. *Sensitivity of the effective growth-rate estimation to temporal re-referencing. Experimental oscillations (red) are compared with calculated oscillations (blue) using the same assumed effective growth rate of 1.031 μm h^{-1} and Shift = 11500 s (upper) or 12678 s (lower). Despite a re-referencing difference of approximately two interference periods, very similar long-duration agreement is retained.*

Alt text:

A temporal re-referencing test compares two phase alignments separated by about two interference periods at the same effective growth rate. Similar multi-hour agreement is retained, showing that the fitted rate is not determined by one initial phase alignment.

S2. HRXRD analysis

S2.1 Quantitative analysis of the split satellite peaks

To quantify the high-order satellite splitting, the +21 and +22 satellites of L1905 were analysed on a linear intensity scale using two-component Gaussian fitting, with the corresponding L1907 satellites fitted by single

Gaussians for comparison (Fig. S5). The fitted L1905 component separations are approximately 11.23 ± 0.64 and 10.81 ± 0.43 arcsec, respectively, with the uncertainties propagated from the fitted peak-centre uncertainties. Although a slight increase in separation with satellite order would be expected for a fixed difference in effective periodicity, the difference between the two fitted values is comparable to the peak-position uncertainty and therefore does not provide evidence for a resolved order dependence.

The fitted L1905 components retain relatively narrow linewidths, with FWHM values of approximately 7.3–10.2 arcsec, comparable to the ~8.9 arcsec FWHM of the unsplit L1907 peaks. These results are consistent with resolved components arising from slightly different effective periodicities, rather than uniform broadening of a single diffraction peak.

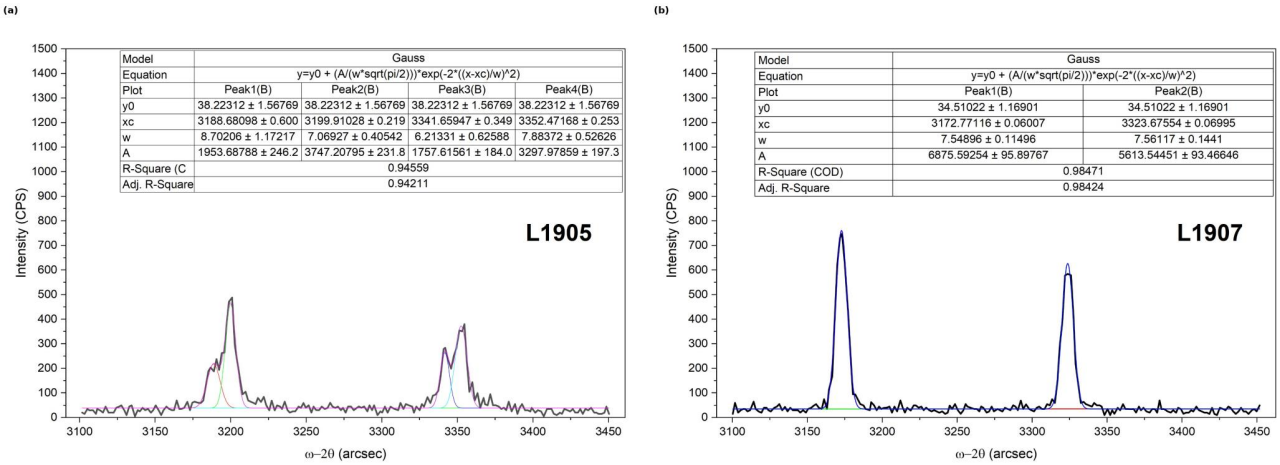


Figure S5. *Gaussian fits to the +21 and +22 HRXRD satellite peaks of (a) L1905 and (b) L1907, plotted on a linear intensity scale. The L1905 satellites are represented by two Gaussian components, whereas the corresponding L1907 satellites are described by single Gaussians.*

Alt text:

Gaussian fits to the positive twenty-first and positive twenty-second HRXRD satellites show two resolved components for L1905 but single peaks for L1907. The resolved L1905 components support the presence of two slightly different effective periodicities.

The Gaussian analysis of the +21 and +22 satellites is used to demonstrate and quantify the resolved high-order splitting. The effective periodicities reported in the main text, however, are determined independently using the well-defined unsplit −1 satellite as a common low-order reference together with the two resolved components of the +27 satellite. This larger angular baseline gives effective periods of approximately 124.58 and 125.03 nm, corresponding to a separation of approximately 0.45 nm (~0.36%).

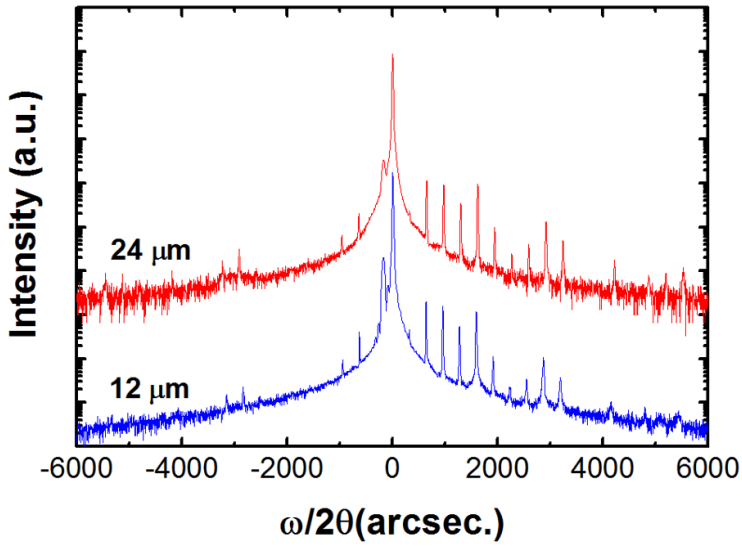


Figure S6. *HRXRD ω–2θ scans of separate 12- and 24-μm GaAs/AlGaAs THz QCL structures with the same nominal active-region design. The curves are vertically offset for clarity. Both structures retain well-resolved high-order satellite features.*

Alt text:

HRXRD scans of a separate THz QCL pair with active-region thicknesses of approximately 12 and 24 micrometres both retain well-resolved high-order satellites. Extended growth under growth-rate-compensated conditions therefore does not necessarily produce pronounced satellite broadening.

S2.2 HRXRD reference for extended growth under growth-rate compensation

To provide an additional reference for long-duration growth, Fig. S6 shows HRXRD scans from a separate pair of THz QCL structures based on the active-region design reported in Ref. [3], which differs from that examined in Fig. 2 of the main manuscript. Within this pair, the two samples have the same nominal active-region design but different active-region thicknesses of approximately 12 and 24 μm. The two samples were grown at different times under nominally identical conditions, using the same pre-growth calibration and growth-rate-compensation procedures described in Ref. [1]. Despite the approximately twofold difference in active-region thickness, both structures retain well-resolved high-order satellite features.

This comparison provides a reference showing that prolonged THz QCL growth under growth-rate-compensated conditions does not necessarily result in pronounced high-order satellite broadening.

S3. Additional device-performance measurements

Figures S7 and S8 present the temperature-dependent light-current-voltage (LIV) characteristics of the 150 μm × 2 mm and 150 μm × 2.5 mm matched L1905/L1907 devices listed in Table I of the main manuscript, providing the underlying experimental data for these two matched-device comparisons.

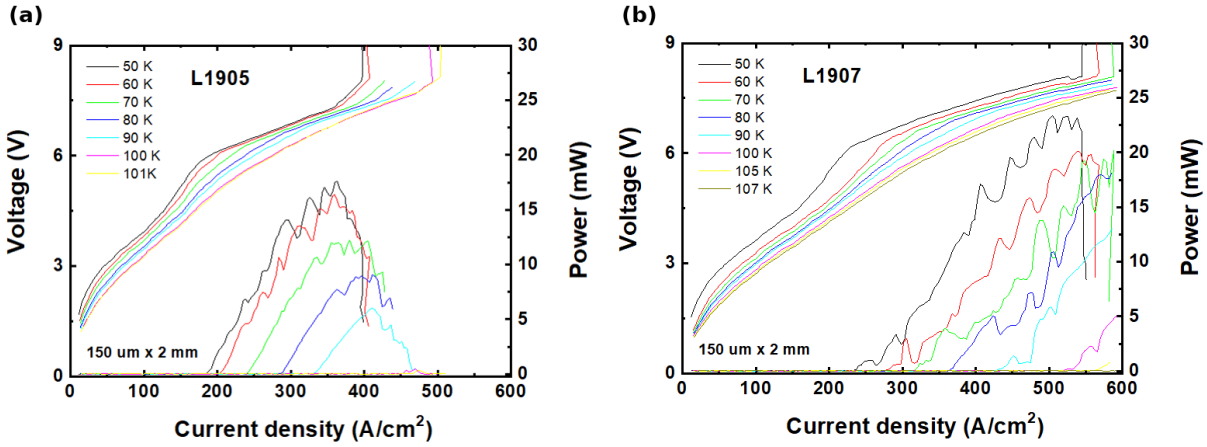


***Figure S7**. Temperature-dependent LIV characteristics of matched 150 µm × 2 mm ridge devices fabricated from (a) L1905 and (b) L1907.*

Alt text:

Temperature-dependent light-current-voltage curves compare matched devices with dimensions of 150 micrometres by 2 millimetres. L1907 sustains lasing over a wider current-density interval, reaches higher peak power, and operates to about 107 kelvin, compared with about 101 kelvin for L1905.

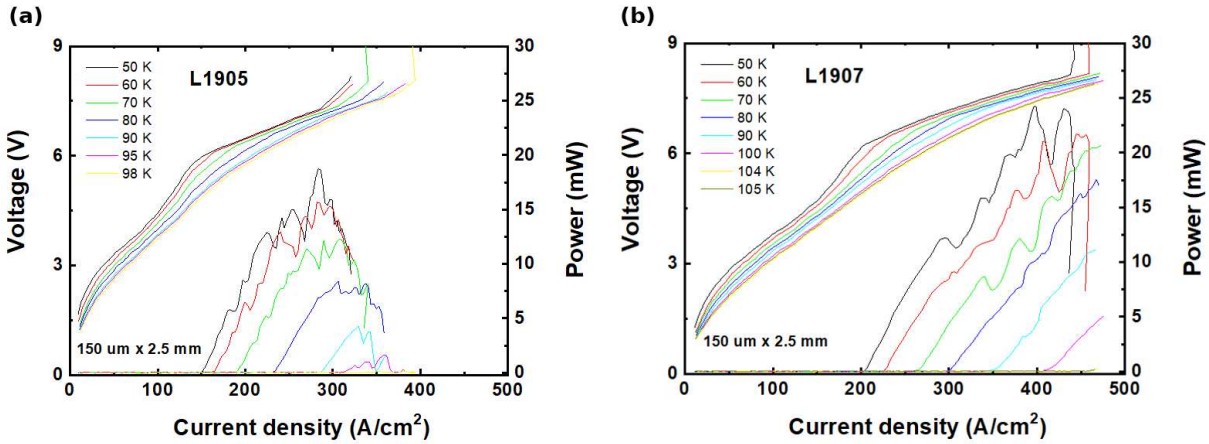


***Figure S8**. Temperature-dependent LIV characteristics of matched 150 µm × 2.5 mm ridge devices fabricated from (a) L1905 and (b) L1907.*

Alt text:

Temperature-dependent light-current-voltage curves compare matched devices with dimensions of 150 micrometres by 2.5 millimetres. L1907 has a broader operating interval, higher maximum current density and peak power, and operates to about 105 kelvin, compared with about 98 kelvin for L1905.

Supplementary References

[1] L. H. Li, J. X. Zhu, L. Chen, A. G. Davies, and E. H. Linfield, "The MBE growth and optimization of high performance terahertz frequency quantum cascade lasers," Optics Express 23, 2720–2729 (2015).

[2] W. G. Breiland and K. P. Killeen, "A virtual interface method for extracting growth rates and high temperature optical constants from thin semiconductor films using in situ normal incidence reflectance," Journal of Applied Physics 78, 6726–6736 (1995).

[3] L. H. Li, L. Chen, J. R. Freeman, M. Salih, P. Dean, A. G. Davies, and E. H. Linfield, “Multi-Watt high power terahertz frequency quantum cascade lasers,” Electronics Letters 53, 799–800 (2017).